Structural systematics in the isomorphous binary co-crystal solvates comprising 2,2'-dithiodibenzoic acid, 4-halobenzoic acid and dimethylformamide (1:1:1), for halide = chloride, bromide and iodide†

Sang Loon Tan, Kong Mun Lo, Yee Seng Tan and Edward R. T. Tiekink*

Research Centre for Crystalline Materials, School of Medical and Life Sciences, Sunway University, 47500 Bandar Sunway, Selangor Darul Ehsan, Malaysia

E-mail: edwardt@sunway.edu.my (ERTT)

TABLE OF CONTENTS

matching, given as a percentage, on the measured PXRD patterns was by Rietveld refinement. The quality of the profile fitting is indicated by the weighted *R*-factor and goodness-of-fit (*S*) in the corresponding plots. Please note that the label "2M" refers to co-former DTBA.DMF.

ESI Figure 3. The TGA thermograms for (a) **1** (b) **2** and (c) **3**. There are three steps for each thermogram:

1: Onset temperature 116.8 °C, weight loss, 9.1%, calculated weight loss for DMF, 13.7%; 182.6 °C, 29.1%, calculated weight loss for 4-**Cl**BA, 29.3%; 301.5 °C, 56.7%, calculated weight loss for DTBA, 57.3%.

2: Onset temperature 119.3 °C, weight loss, 12.2%, calculated weight loss for DMF, 12.6%; 195.6 °C, 34.2%, calculated for 4-**Br**BA, 34.6%; 299.6 °C, 50.6%, calculated for DTBA, 52.8%.

3: Onset temperature 101.9 °C, weight loss, 10.4%, calculated weight loss for DMF, 11.7%; 203.1 °C, 37.8.1%, calculated for 4-**I**BA, 39.5%; 298.9 °C, 48.1%, calculated for DTBA, 48.8%.

ESI Figure 4. The DSC traces for (a) **1** (b) **2** and (c) **3**. The red trace is the heating cycle and the blue, the cooling cycle.

ESI Figure 5. Images of the thermo-microscopic study for (a) **1** [left-hand image: crystal at room temperature; central image: onset of desolvation with loss of transparency at 143 °C; and right-hand image: crystal melting at 162 °C] (b) **2** [desolvation: 211 °C; melting: 284 °C] and (c) **3** [desolvation: 215 °C; melting: 267 °C].

ESI Figure 6. The molecular structures of **2** (upper view) and **3** showing atom-labelling scheme and displacement parameters at the 70% probability level. The dashed lines indicate hydrogen bonds.

ESI Figure 7. Images of the molecular packing in **3**: (a) supramolecular aggregation leading to a tape along the *b*-axis and (b) view of the unit-cell contents in projection down the *b*-axis. The intermolecular contacts are represented by dashed lines: O–H···O (red), C–H···S (blue), C–H···O (plum), C–H···π (brown), C–O···π (pink) and π···π(green). In (a), one C7–H7···O4 interaction been indicated by an asterisk and in (b) one each of the C23–H23b···O5 and C18–H18···S2 interactions has been indicated by an asterisk – these are absent in the packing of each of **1** and **2**.

ESI Figure 8. The MEP mapped on the Hirshfeld surfaces of **1**-**3**, showing the electrostatic potential charge on selected atoms for 4-**X**BA, DTBA and DMF for (a) **1**, (b) **2** and (c) **3**.

ESI Figure 9. A comparison of the molecular packing between (a) **1** (red) and **2** (blue), (b) **1** and **3** (green) and (c) **2** and **3**, highlighting all sets of molecules are fitted within the 20% tolerance criteria in both distance and angle deviations.

ESI Figure 10. (a) The dendrogram showing the packing similarity with number of non-overlapped molecules as indexed by the corresponding colour code for **1**-**3**, with dark-green indicating almost identical packing while dark-red indicates the opposite and (b) the similarity matrix showing the quantitative similarity indices across crystals **1**-**3**.

ESI Figure 11. Two perspective views of d_{norm} mappings within the property range of -0.0595 to 1.0429 arbitrary units for the individual components of the binary co-crystal solvates for (a) DTBA, (b) DMF, (c) 4-**Cl**BA, (d) 4-**Br**BA and (e) 4-**I**BA.

ESI Figure 12. The Hirshfeld surface mapped with curvedness (property range: −4.0 to +0.4 arbitrary units; left) and shape index (property range: −1.0 to +1.0 arbitrary units; right) for **1**-**3**, showing the shape complementarity between the quasi π-hole of $\{\cdots HOC{=}O\}_2$ and the (a) Cl, (b) Br and (c) I atoms.

ESI Figure 13. Non-covalent interaction (NCI) plot showing the iso-surface of the reduced density gradient resulting from the C–X···quasi-π[$\{\cdots HOC{=}O\}_2$] interaction for (a) X = Cl, (b) X = Br and (c) X = I. The iso-surfaces are coloured according to the values of electron density, with green indicative of weak attraction, while blue and red are indicative of strong attraction and strong repulsion, respectively. The cut-off value is set at RDG = 0.5 a.u. and colour scale is within -0.4 < ρ < 0.4 a.u.

ESI Figure 14. Overall (top) and decomposed fingerprint (H···H, H···O/O···H, H···C/C···H and H···S/S···H) plots delineated into the corresponding specific contacts for the individual components in (a) **1**, (b) **2** and (c) **3**.

ESI Figure 15. The distribution of calculated surface contacts and associated enrichment ratios for the individual components (rows) of **1**-**3** (columns).

ESI Figure 16. Non-covalent interaction (NCI) plot showing the iso-surface of the reduced density gradient resulting from the C24···X interactions in (a) **1**, (b) **2** and (c) **3**. The iso-surface is coloured according to the values of electron density, with green indicative of weak attraction, while blue and red are indicative of strong attraction and strong repulsion, respectively. The cut-off value is set at RDG = 0.5 a.u. and colour scale is within -0.4 < ρ < 0.4 a.u.

ESI Figure 17. Perspective views of the electrostatic energy framework (left column), dispersion force (middle column) and overall energy framework (right

column) for **1** (top row), **2** (middle row) and **3** (bottom row). The cylindrical radius is proportional to the relative strength of the corresponding energies and adjusted to the same scale factor of 100 with a cut-off value of 8 kJ/mol within a 2 × 2 × 1 unit-cells.

ESI Table 1. Selected geometric parameters (Å, º) for **1**-**3**.

Parameter	**1**	**2**	**3**
C1–O1	1.2236(17)	1.225(2)	1.227(3)
C1–O2	1.3182(17)	1.318(2)	1.315(3)
C8–O3	1.2278(17)	1.225(2)	1.230(3)
C8–O4	1.3166(17)	1.322(2)	1.318(3)
C21–O5	1.2199(17)	1.220(2)	1.220(3)
C21–O6	1.3179(17)	1.320(2)	1.319(3)
(C1,O1,O2)/(C2-C7)	4.88(9)	4.81(12)	3.85(17)
C14–S1–S2–C15	-94.48(6)	-94.64(8)	-94.22(11)
(C9-C14)/(C15-C20)	77.81(5)	78.25(5)	78.82(7)
(C8,O3,O4)/(C9-C14)	16.04(11)	13.44(10)	14.04(15)
(C20,O5,O6)/(C15-C20)	13.29(8)	15.92(13)	15.72(17)

ESI Table 2 A summary of the geometric parameters (Å, º) characterising the key intermolecular contacts (A–H···B) in the crystals of **2** and **3**.

Contact	H···B	A···B	A–H···B	Symmetry operation
2				
O2–H2o···O3	1.81(2)	2.6491(18)	176.4(17)	*x*, *y*, *z*
O4–H4o···O1	1.78(2)	2.6161(18)	175(3)	*x*, *y*, *z*
O6–H6o···O7	1.74(2)	2.5734(19)	176(2)	*x*, *y*, *z*
C22–H22···O5	2.38	3.136(2)	136	*x*, *y*, *z*
C13–H13···O7	2.58	3.353(2)	139	1-*x*, 1-*y*, 2-*z*
C11–H11···S1	2.79	3.4723(16)	129	*x*, -1+*y*, *z*
C22–O7···Cg(C15-C20)	3.8671(15)	3.5189(17)	64.65(9)	1-*x*, 1-*y*, 2-*z*
C24–H24b···Cg(C15-C20)	2.86	3.531(2)	127	1-*x*, 1-*y*, 2-*z*
Cg(C2–C7) ···Cg(C9-C14)	–	3.7787(10)	6.86(8)	1-*x*, 1-*y*, 1-*z*
Cg(C2–C7) ···Cg(C2-C7)	–	3.8150(10)	0	2-*x*, 2-*y*, 1-*z*
C17–H17···Cg(C9-C14)	2.89	3.8365(18)	176	-1+*x*, *y*, *z*
3				
O2–H2o···O3	1.82(3)	2.655(2)	175(2)	*x*, *y*, *z*
O4–H4o···O1	1.78(3)	2.618(2)	178(3)	*x*, *y*, *z*
O6–H6o···O7	1.74(3)	2.570(2)	178(4)	*x*, *y*, *z*
C22–H22···O5	2.40	3.156(3)	136	*x*, *y*, *z*
C13–H13···O7	2.59	3.384(3)	141	1-*x*, 1-*y*, 2-*z*
C11–H11···S1	2.78	3.484(2)	132	*x*, -1+*y*, *z*
C22–O7···Cg(C15-C20)	3.8293(18)	3.490(3)	65.00(12)	1-*x*, 1-*y*, 2-*z*

C24-H24b···Cg(C15-C20)	2.89	3.567(3)	127	1-*x*, 1-*y*, 2-*z*
Cg(C2-C7)···Cg(C9-C14)	–	3.8365(18)	8.89(11)	1-*x*, 1-*y*, 1-*z*
Cg(C2-C7)···Cg(C2-C7)	–	3.8286(14)	0	2-*x*, 2-*y*, 1-*z*
C18–H18···S2	2.84	3.441(2)	122	-1+*x*, *y*, *z*
C23–H23b···O5	2.58	3.453(3)	149	2-*x*, 2-*y*, 2-*z*
C7–H7···O4	2.60	3.371(3)	139	*x*, 1+*y*, *z*

ESI Table 3 Interaction energies (kJ/mol) for identified close contacts present in the crystals of **1-3**.

Close contact	$E_{electrostatic}$	$E_{polarization}$	$E_{dispersion}$	$E_{repulsion}$	E_{total}	Symmetry operation
1						
O2–H2o···O3 + O4–H4o···O1	-140.7	-21.7	-11.5	103.0	-70.9	*x*, *y*, *z*
O6–H6o···O7 + C22–H22···O5	-100.0	-16.6	-9.5	66.2	-59.9	*x*, *y*, *z*
C13–H13···O7	-5.3	-3.6	-26.9	11.9	-23.9	1-*x*, 1-*y*, 1-*z*
C11–H11···S1 + C11–H11···O3	-13.8	-1.6	-14.5	17.5	-12.6	*x*, -1+*y*, *z*
π(C2-C7)···π(C9-C14)	-0.5	-0.7	-34.4	17.3	-18.4	1-*x*, 1-*y*, -*z*
π(C2-C7)···π(C2-C7)	-18.5	-0.6	-33.6	23.2	-29.6	2-*x*, 2-*y*, -*z*
C6–H6···O1	-9.2	-1.3	-5.2	3.4	-12.2	*x*, 1+*y*, *z*
C10–H10···O2 + C7–H7···O4	-1.9	-0.7	-11.5	8.0	-6.1	*x*, 1+*y*, *z*
C19–H19···C19	-2.6	-0.3	-13.7	9.1	-7.5	-*x*, 1-*y*, 1-*z*
C18–H18···S2 + C17–H17···C13 + C17–H17···C14	-10.0	-1.5	-20.9	15.8	-16.7	-1+*x*, *y*, *z*
C23–H23b···O5	-9.7	-1.5	-8.7	5.9	-14.0	2-*x*, 2-*y*, 1-*z*
C24···Cl	-2.0	-0.2	-5.3	3.8	-3.7	*x*, *y*, 1+*z*
2						
O2–H2o···O3 + O4–H4o···O1	-140.4	-21.4	-11.3	-101.7	-71.5	*x*, *y*, *z*

O6–H6o···O7 +	-99.4	-16.5	-9.4	66.4	-58.9	*x*, *y*, *z*
C22–H22···O5						
C13–H13···O7	-5.0	-3.6	-27.0	11.8	-23.7	1-*x*, 1-*y*, 1-*z*
C11–H11···S1 +	-13.7	-1.6	-14.5	17.3	-12.4	*x*, -1+*y*, *z*
C11–H11···O3						
π(C2-C7)···π(C9-C14)	-0.8	-0.7	-35.3	17.4	-19.4	1-*x*, 1-*y*, -*z*
π(C2-C7)···π(C2-C7)	-18.4	-0.6	-35.4	24.0	-30.4	-1+*x*, -1+*y*, *z*
C6–H6···O1	-9.4	-1.3	-6.0	3.9	-12.9	*x*, 1+*y*, *z*
C10–H10···O2 +	-2.3	-0.7	-11.5	8.0	-6.6	*x*, 1+*y*, *z*
C7–H7···O4						
C19–H19···C19	-2.7	-0.3	-13.5	8.7	-7.9	-*x*, 1-*y*, 1-*z*
C18–H18···S2 +	-10.4	-1.5	-20.5	15.8	-16.6	-1+*x*, *y*, *z*
C17–H17···C13 +						
C17–H17···C14						
C23–H23c···O5	-9.5	-1.5	-8.5	5.8	-13.7	-*x*, -*y*, 1-*z*
C24···Br	-3.1	-0.2	-6.4	5.7	-4.0	*x*, *y*, 1+*z*
3						
O2–H2o···O3 +	-140.7	-21.5	-11.3	100.4	-73.2	*x*, *y*, *z*
O4–H4o···O1						
O6–H6o···O7 +	-100.2	-16.7	-9.3	66.3	-59.9	*x*, *y*, *z*
C22–H22···O5						
C13–H13···O7	-4.8	-3.6	-27.0	11.6	-23.6	1-*x*, 1-*y*, 2-*z*
C11–H11···S1 +	-13.0	-1.5	-13.9	16.1	-12.4	*x*, -1+*y*, *z*
C11–H11···O3						
π(C2-C7)···π(C9-C14)	-1.6	-0.7	-35.4	-17.4	-20.2	1-*x*, 1-*y*, -*z*

π(C2-C7)···π(C2-C7)	-19.1	-0.6	-36.2	24.8	-31.3	-1+*x*, 1+*y*, *z*
C6–H6···O1	-10.0	-1.3	-7.2	4.9	-13.7	*x*, 1+*y*, *z*
C10–H10···O2 + C7–H7···O4	-2.4	-0.7	-11.8	8.3	-6.7	*x*, 1+*y*, *z*
C19–H19···C19	-2.5	-0.3	-13.4	8.1	-8.1	-*x*, 1-*y*, 2-*z*
C18–H18···S2 + C17–H17···C13 + C17–H17···C14	-10.4	-1.6	-19.2	15.4	-15.6	-1+*x*, *y*, *z*
C23–H23b···O5	-9.4	-1.5	-8.1	5.6	-13.5	2-*x*, 2-*y*, 2-*z*
C24···I	-4.9	-0.2	-7.7	9.0	-3.8	*x* ,*y*, 1+*z*

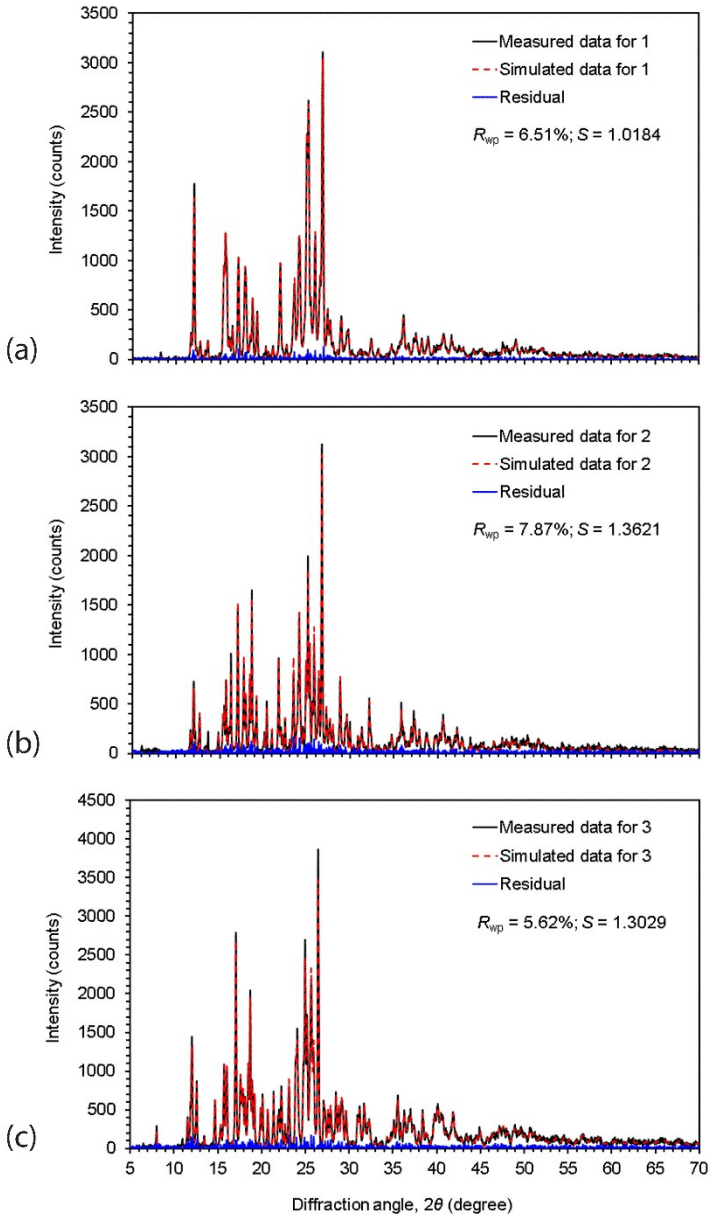

ESI Figure 1. The measured and simulated PXRD patterns for (a) **1**, (b) **2** and (c) **3**. PXRD pattern fitting of the experimental (dark line) and simulated profiles (dashed red line) by Rietveld refinement along with the residual plot (blue line). The quality of the profile fitting is indicated by the weighted *R*-factor and goodness-of-fit in the corresponding plots.

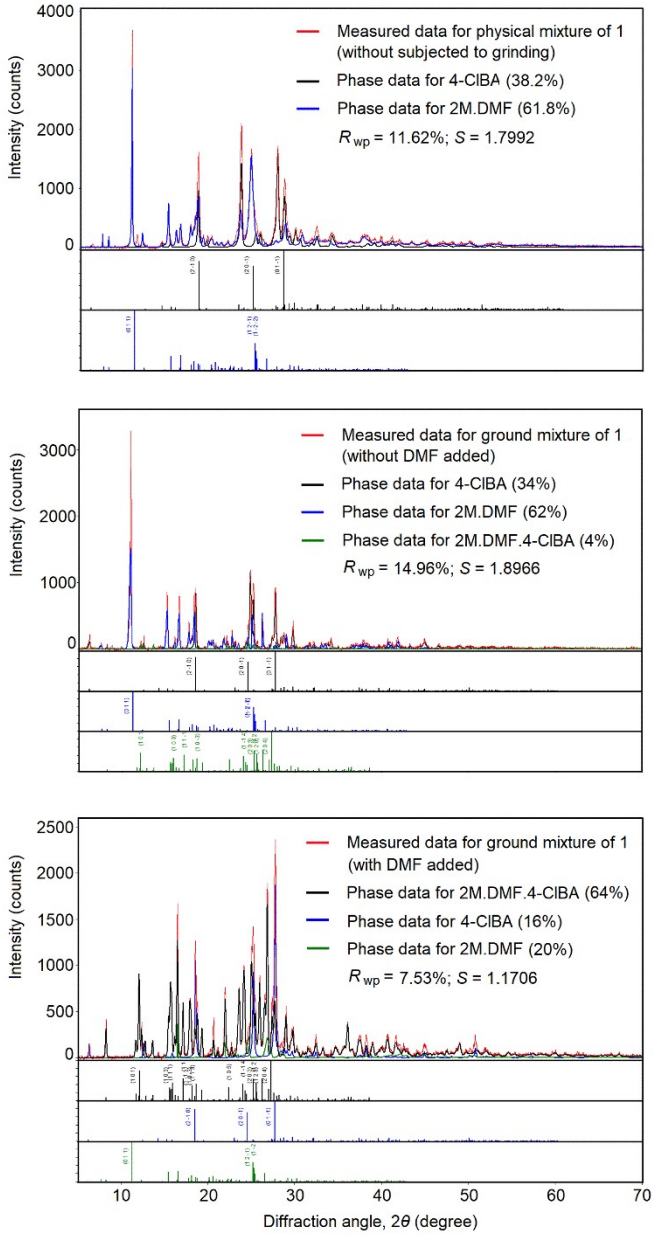
Measured data for physical mixture of 1 (without subjected to grinding)
Phase data for 4-ClBA (38.2%)
Phase data for 2M.DMF (61.8%)
R_{wp} = 11.62%; S = 1.7992
Intensity (counts)
Measured data for ground mixture of 1 (without DMF added)
Phase data for 4-ClBA (34%)
Phase data for 2M.DMF (62%)
Phase data for 2M.DMF.4-ClBA (4%)
R_{wp} = 14.96%; S = 1.8966
Measured data for ground mixture of 1 (with DMF added)
Phase data for 2M.DMF.4-ClBA (64%)
Phase data for 4-ClBA (16%)
Phase data for 2M.DMF (20%)
R_{wp} = 7.53%; S = 1.1706
Diffraction angle, 2θ (degree)

(a)

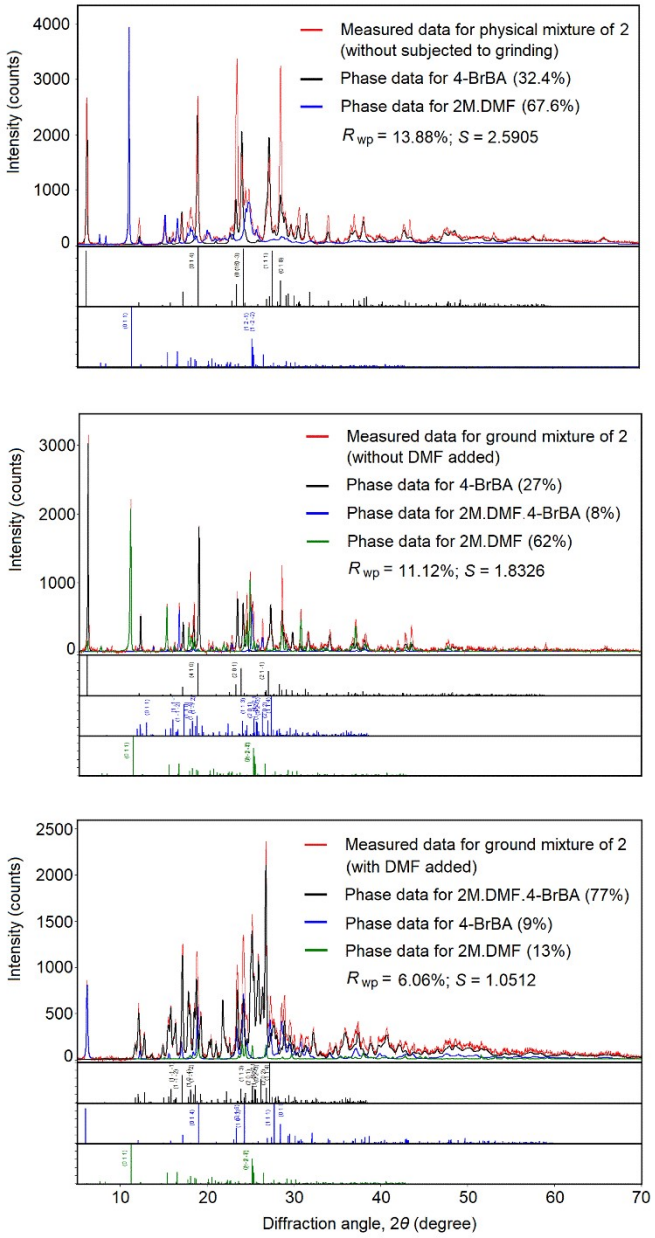
Measured data for physical mixture of 2 (without subjected to grinding)
Phase data for 4-BrBA (32.4%)
Phase data for 2M.DMF (67.6%)
R_{wp} = 13.88%; S = 2.5905
Measured data for ground mixture of 2 (without DMF added)
Phase data for 4-BrBA (27%)
Phase data for 2M.DMF.4-BrBA (8%)
Phase data for 2M.DMF (62%)
R_{wp} = 11.12%; S = 1.8326
Measured data for ground mixture of 2 (with DMF added)
Phase data for 2M.DMF.4-BrBA (77%)
Phase data for 4-BrBA (9%)
Phase data for 2M.DMF (13%)
R_{wp} = 6.06%; S = 1.0512
Intensity (counts)
Diffraction angle, 2θ (degree)

(b)

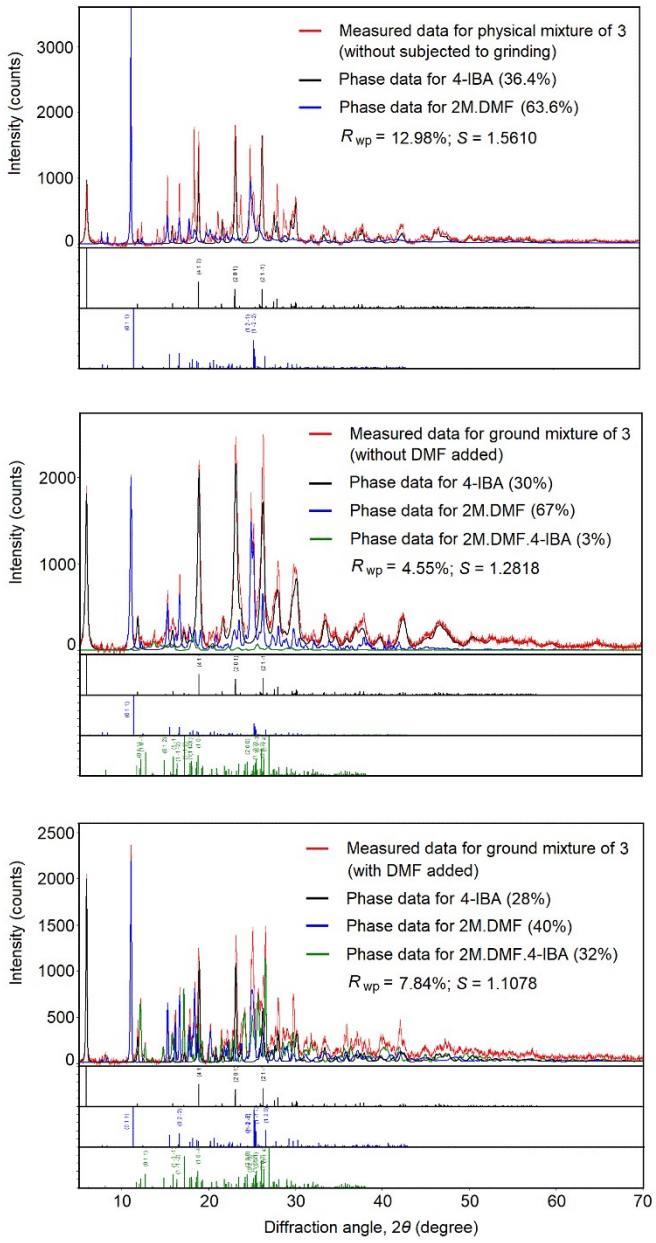

(c)

ESI Figure 2. The measured PXRD patterns on physical mixtures, ground mixtures in the absence and presence of DMF for (a) **1**, (b) **2** and (c) **3**. Phase matching, given as a percentage, on the measured PXRD patterns was by Rietveld refinement. The quality of the profile fitting is indicated by the weighted *R*-factor and goodness-of-fit (*S*) in the corresponding plots. Please note that the label "2M" refers to co-former DTBA.DMF.

Filename: E:\STA Analysis\Is...\2mcl_processed-2.stad
Operator ID: alant
Sample ID: 2MCl
Sample Weight: 5.309 mg
Comment:

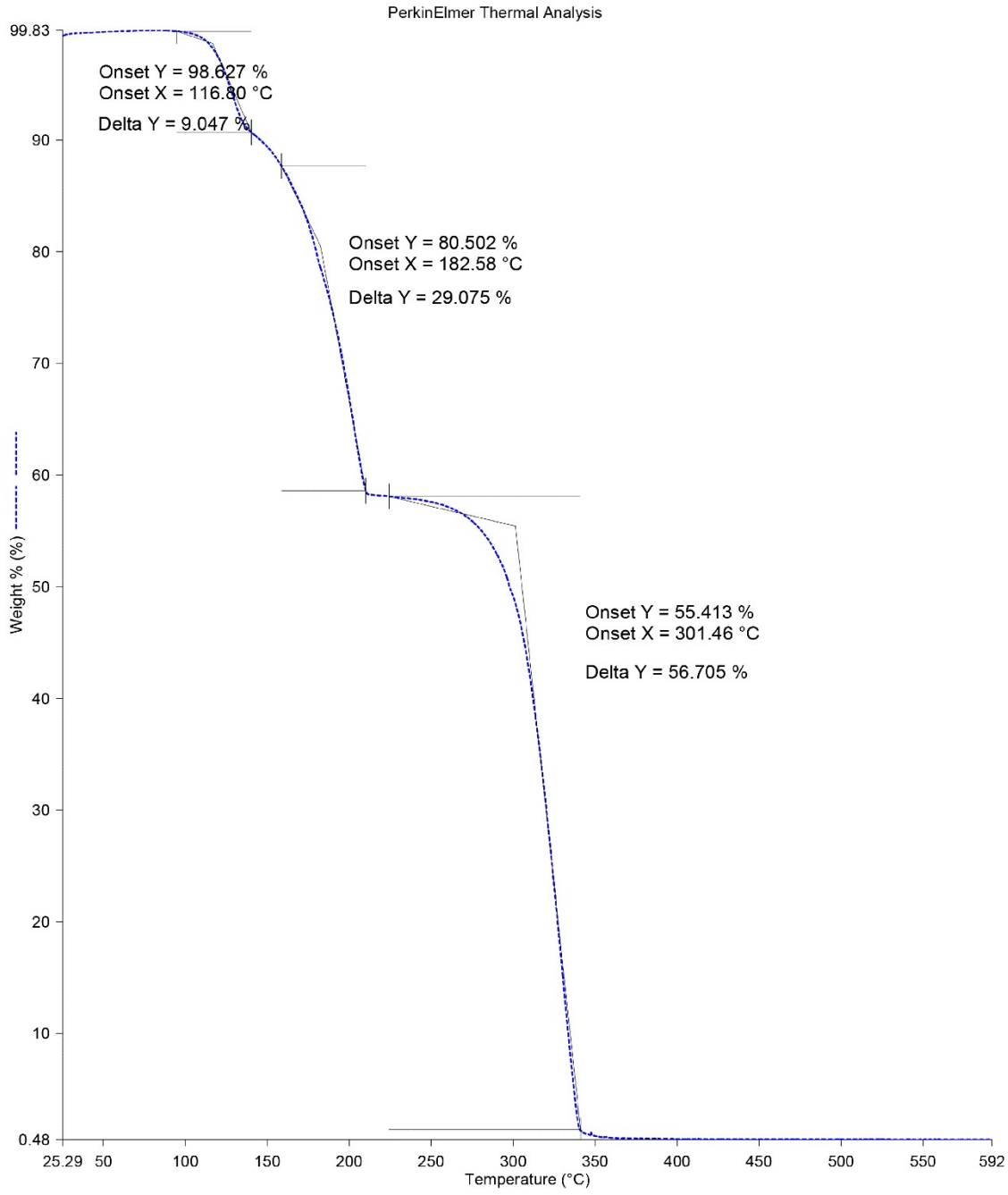

1) Hold for 45.0 min at 25.00°C
2) Heat from 25.00°C to 600.00°C at 10.00°C/min
3) Cool from 600.00°C to 25.00°C at 10.00°C/min
4) Hold for 1.0 min at 25.00°C

(a)

Filename: E:\STA Analysis\Iso Series\2MBr-02.stad
Operator ID: alant
Sample ID: 2MBr-02
Sample Weight: 4.818 mg
Comment:

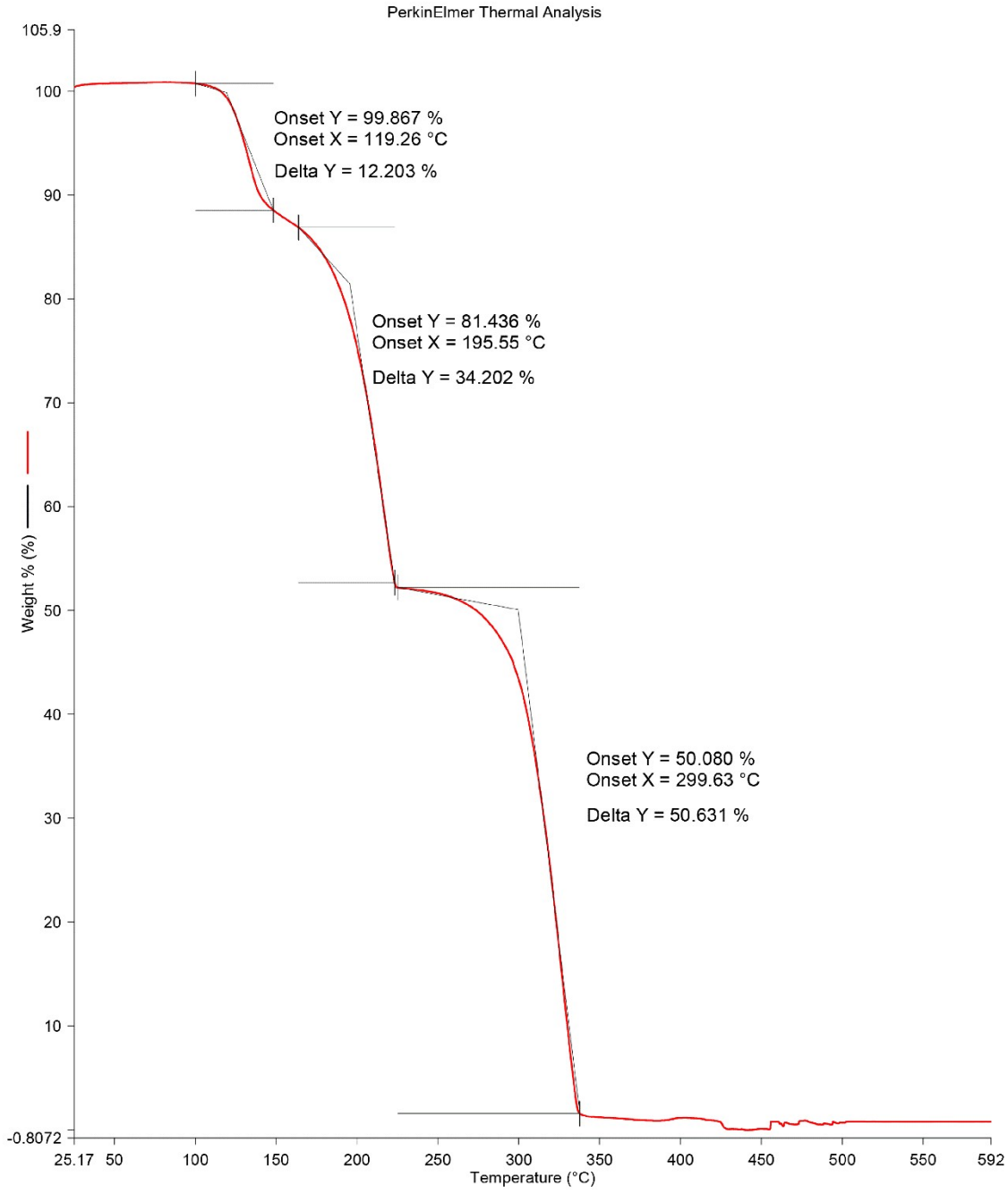

16/4/2021 9:27:07 AM

1) Hold for 45.0 min at 25.00°C
2) Heat from 25.00°C to 600.00°C at 10.00°C/min
3) Cool from 600.00°C to 25.00°C at 10.00°C/min
4) Hold for 1.0 min at 25.00°C

(b)

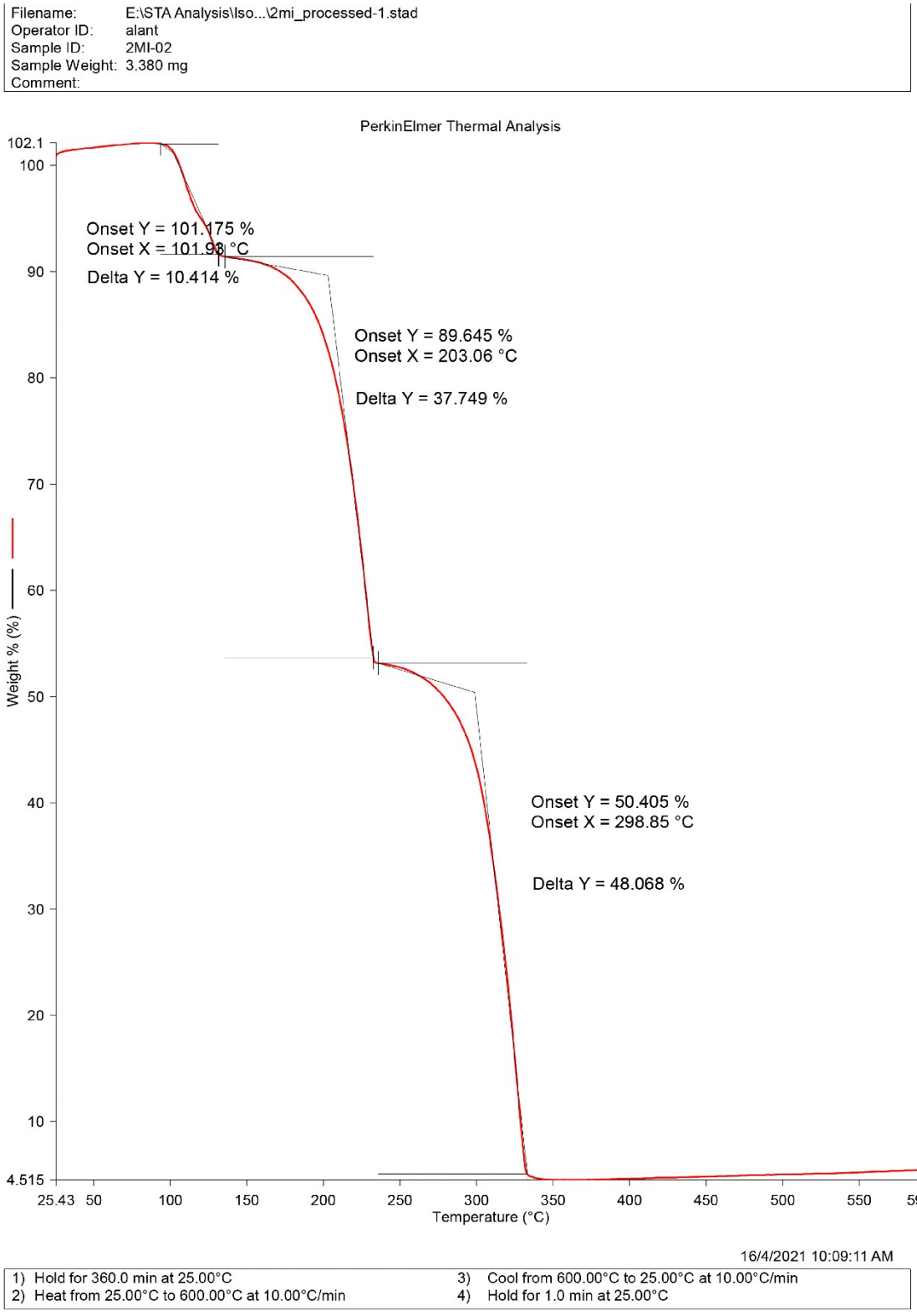

(c)

ESI Figure 3. The TGA thermograms for (a) **1** (b) **2** and (c) **3**. There are three steps for each thermogram:

1: Onset temperature 116.8 °C, weight loss, 9.1%, calculated weight loss for DMF, 13.7%; 182.6 °C, 29.1%, calculated weight loss for 4-**Cl**BA, 29.3%; 301.5 °C, 56.7%, calculated weight loss for DTBA, 57.3%.

2: Onset temperature 119.3 °C, weight loss, 12.2%, calculated weight loss for DMF, 12.6%; 195.6 °C, 34.2%, calculated for 4-**Br**BA, 34.6%; 299.6 °C, 50.6%, calculated for DTBA, 52.8%.

3: Onset temperature 101.9 °C, weight loss, 10.4%, calculated weight loss for DMF, 11.7%; 203.1 °C, 37.8.1%, calculated for 4-**I**BA, 39.5%; 298.9 °C, 48.1%, calculated for DTBA, 48.8%.

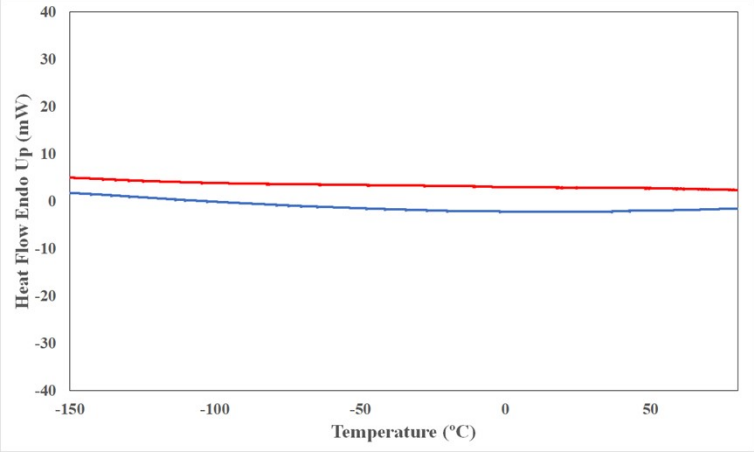

(a)

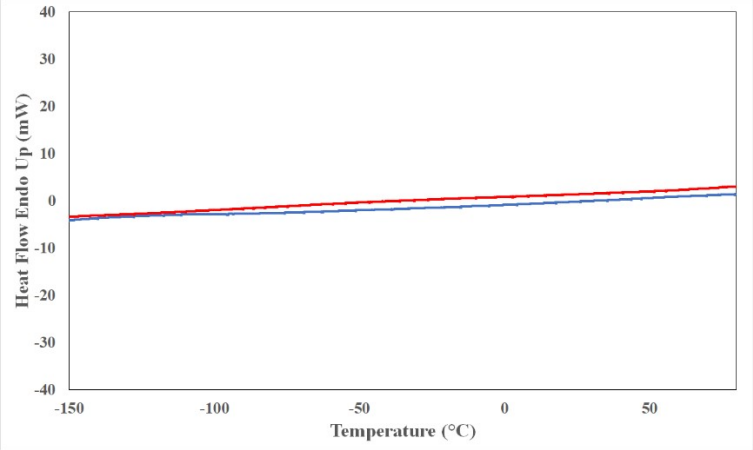

(b)

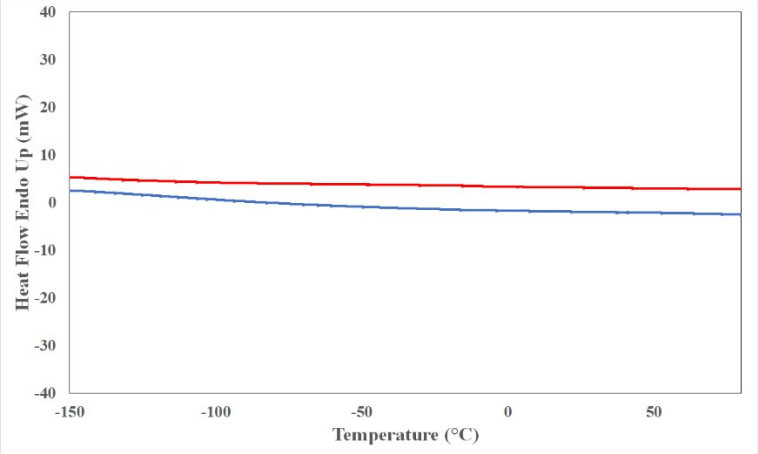

(c)

ESI Figure 4. The DSC traces for (a) **1** (b) **2** and (c) **3**. The red trace is the heating cycle and the blue, the cooling cycle.

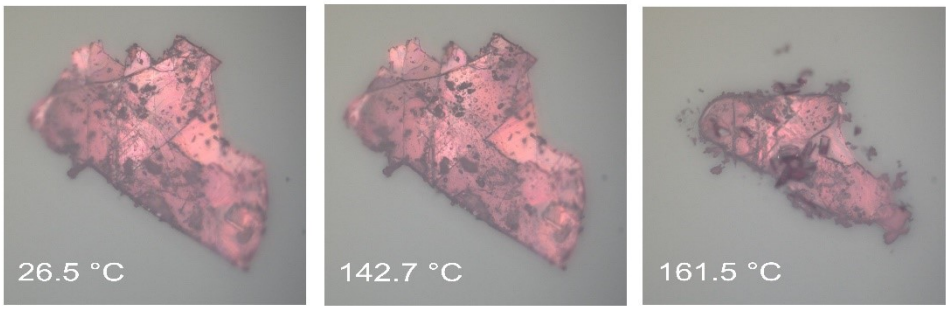

(a)

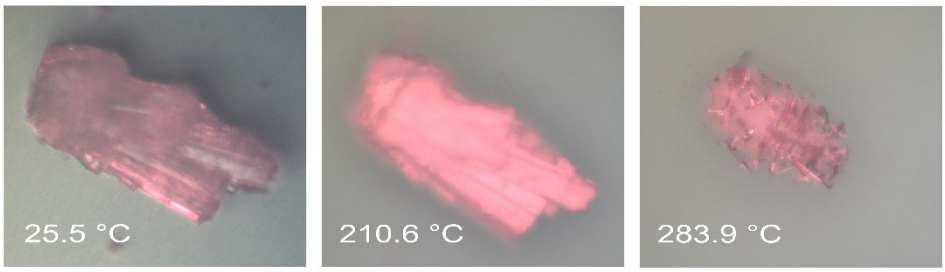

(b)

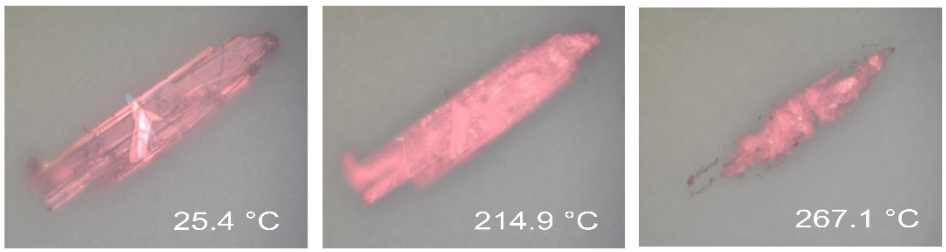

(c)

ESI Figure 5. Images of the thermo-microscopic study for (a) **1** [left-hand image: crystal at room temperature; central image: onset of desolvation with loss of transparency at 143 °C; and right-hand image: crystal melting at 162 °C] (b) **2** [desolvation: 211 °C; melting: 284 °C] and (c) **3** [desolvation: 215 °C; melting: 267 °C].

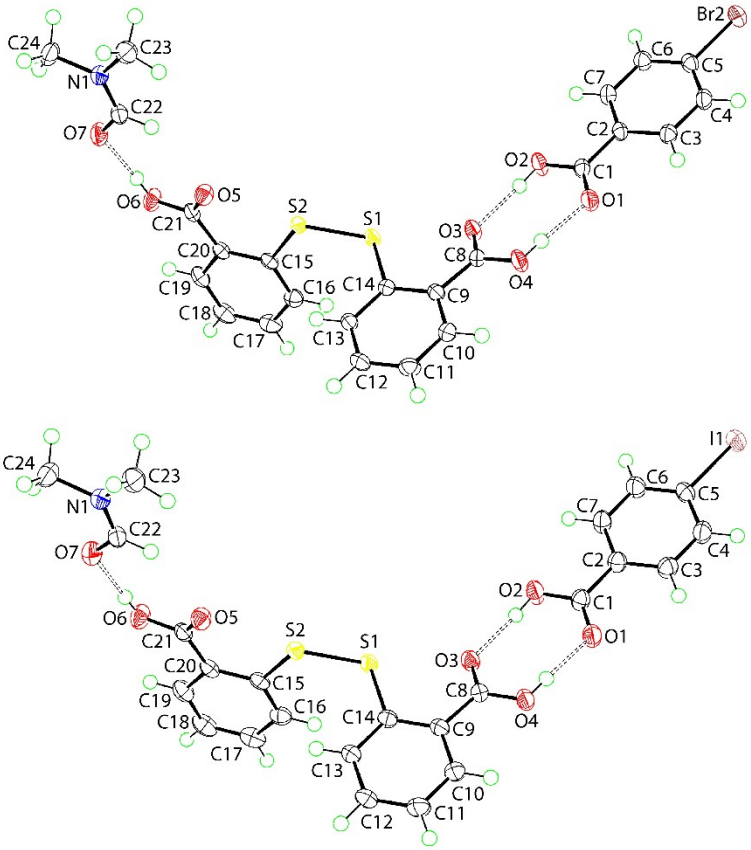

ESI Figure 6. The molecular structures of **2** (upper view) and **3** showing atom-labelling scheme and displacement parameters at the 70% probability level. The dashed lines indicate hydrogen bonds.

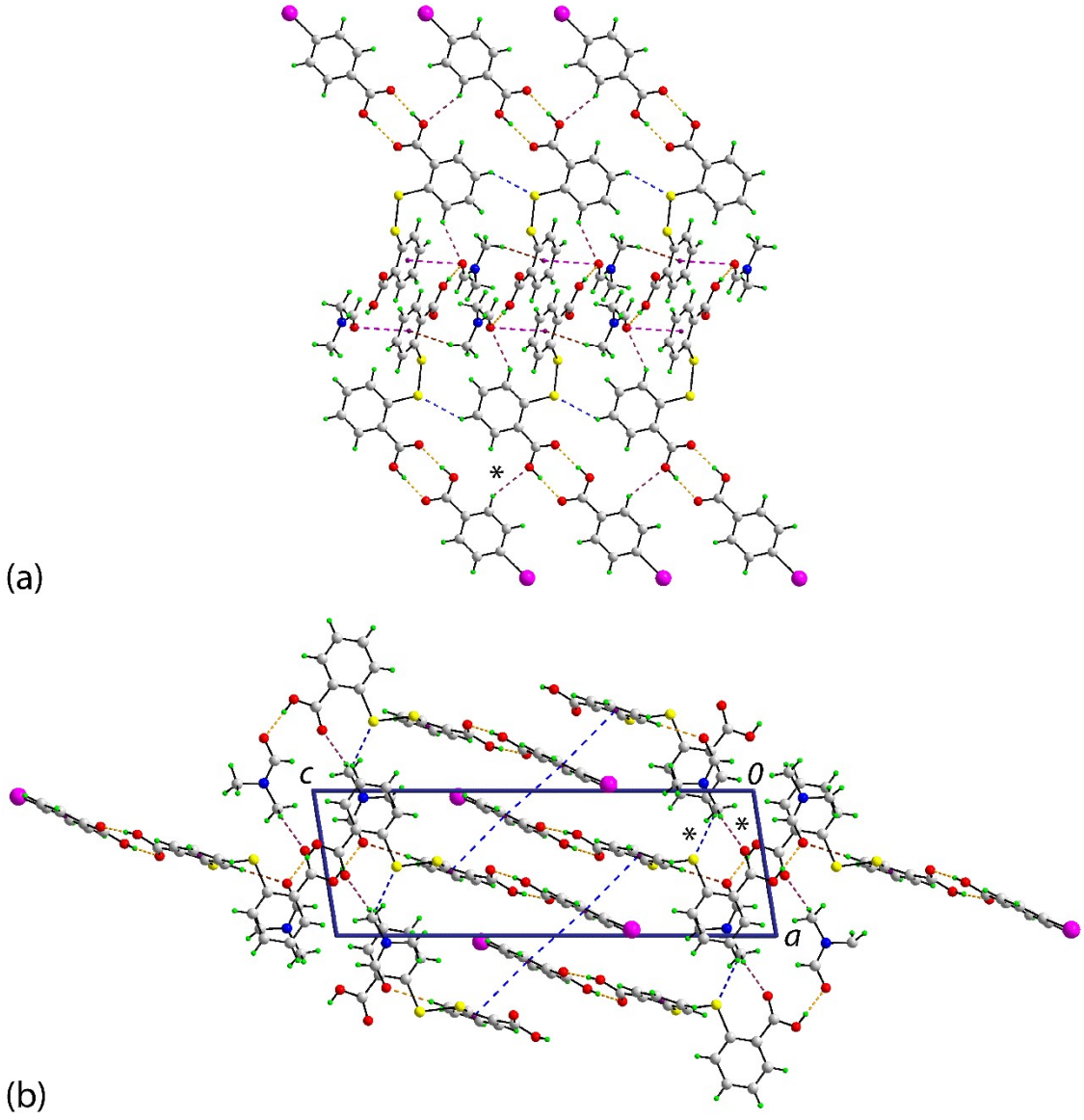

ESI Figure 7. Images of the molecular packing in **3**: (a) supramolecular aggregation leading to a tape along the *b*-axis and (b) view of the unit-cell contents in projection down the *b*-axis. The intermolecular contacts are represented by dashed lines: O–H···O (red), C–H···S (blue), C–H···O (plum), C–H···π (brown), C–O···π (pink) and π···π(green). In (a), one C7–H7···O4 interaction been indicated by an asterisk and in (b) one each of the C23–H23b···O5 and C18–H18···S2 interactions has been indicated by an asterisk – these are absent in the packing of each of **1** and **2**.

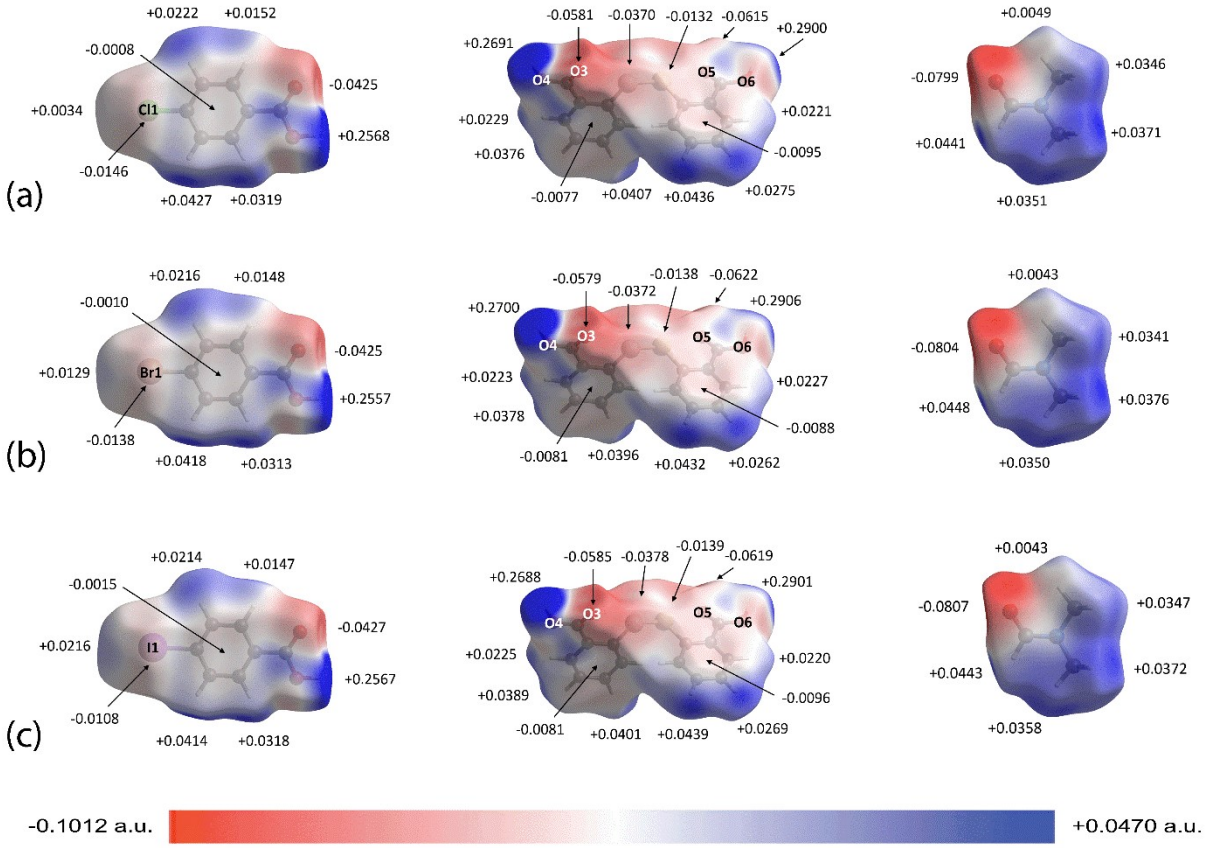

ESI Figure 8. The MEP mapped on the Hirshfeld surfaces of **1**-**3**, showing the electrostatic potential charge on selected atoms for 4-**X**BA, DTBA and DMF for (a) **1**, (b) **2** and (c) **3**.

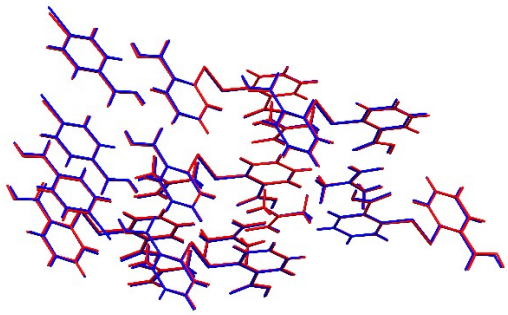

(a)

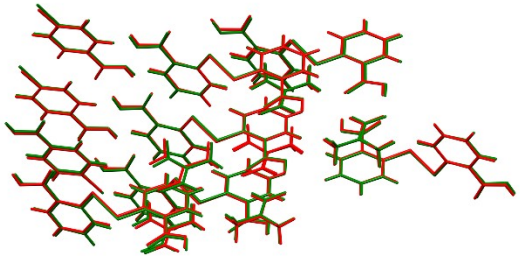

(b)

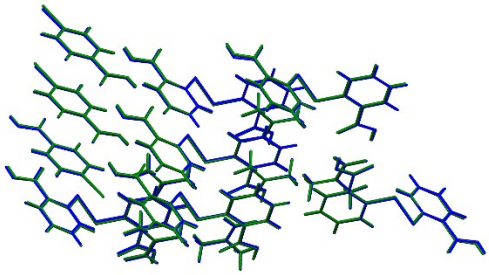

(c)

ESI Figure 9. A comparison of the molecular packing between (a) **1** (red) and **2** (blue), (b) **1** and **3** (green) and (c) **2** and **3**, highlighting all sets of molecules are fitted within the 20% tolerance criteria in both distance and angle deviations.

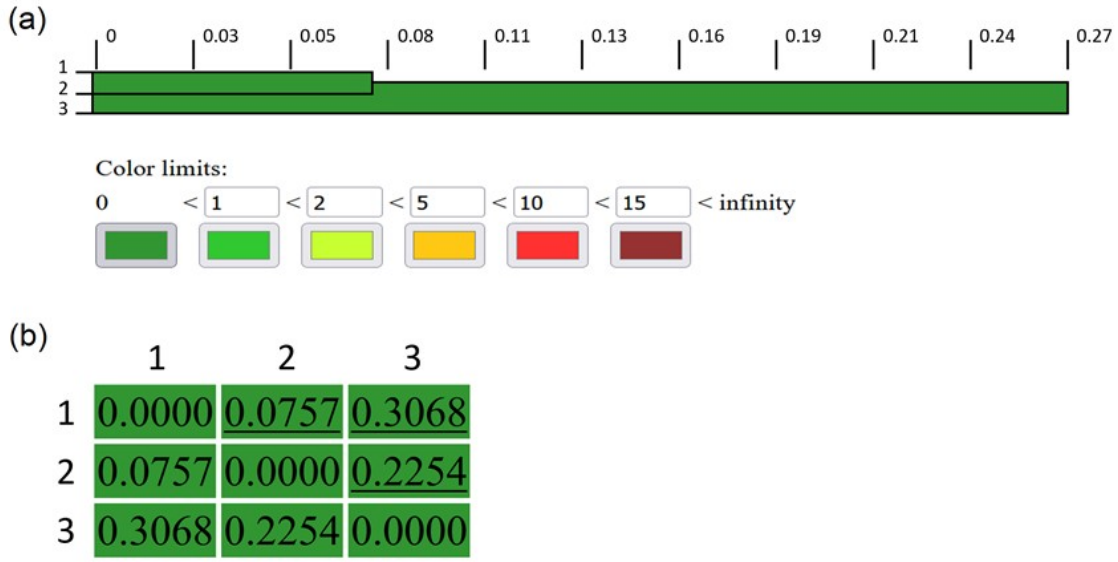

(b)

	1	2	3
1	0.0000	0.0757	0.3068
2	0.0757	0.0000	0.2254
3	0.3068	0.2254	0.0000

ESI Figure 10. (a) The dendrogram showing the packing similarity with number of non-overlapped molecules as indexed by the corresponding colour code for **1**-**3**, with dark-green indicating almost identical packing while dark-red indicates the opposite and (b) similarity matrix showing the quantitative similarity indices across crystals **1**-**3**.

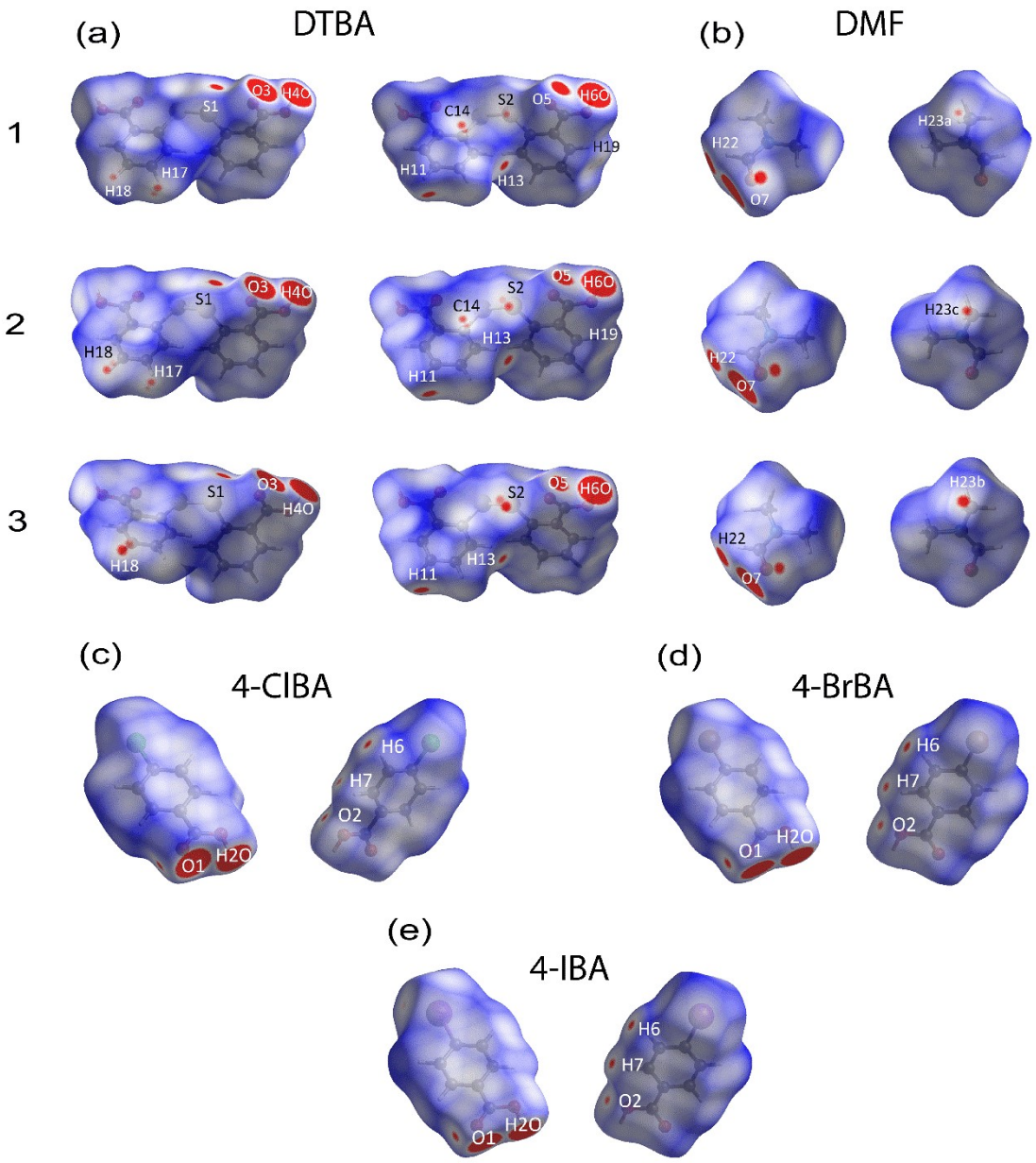

ESI Figure 11. Two perspective views of d_{norm} mappings for **1**-**3** within the property range of -0.0595 to 1.0429 arbitrary units for the individual components of the binary co-crystal solvates for (a) DTBA, (b) DMF, (c) 4-**Cl**BA, (d) 4-**Br**BA and (e) 4-**I**BA.

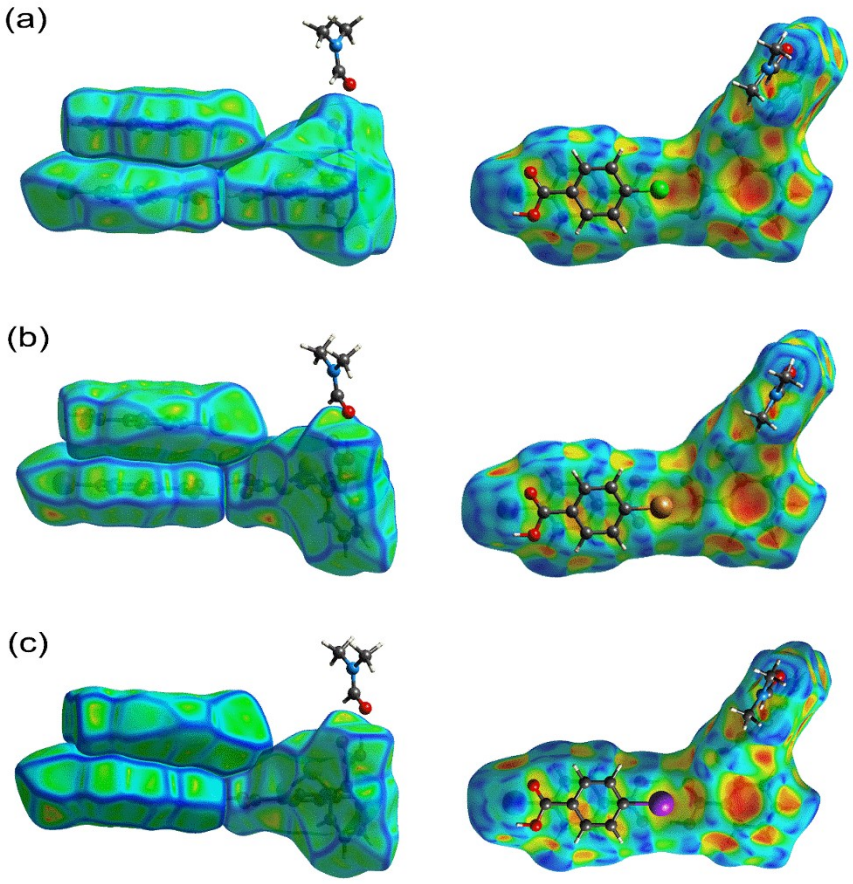

ESI Figure 12. The Hirshfeld surface mapped with curvedness (property range: −4.0 to +0.4 arbitrary units; left) and shape index (property range: −1.0 to +1.0 arbitrary units; right) for **1-3**, showing the shape complementarity between the quasi π-hole of $\{\cdots HOC{=}O\}_2$ and the (a) Cl, (b) Br and (c) I atoms.

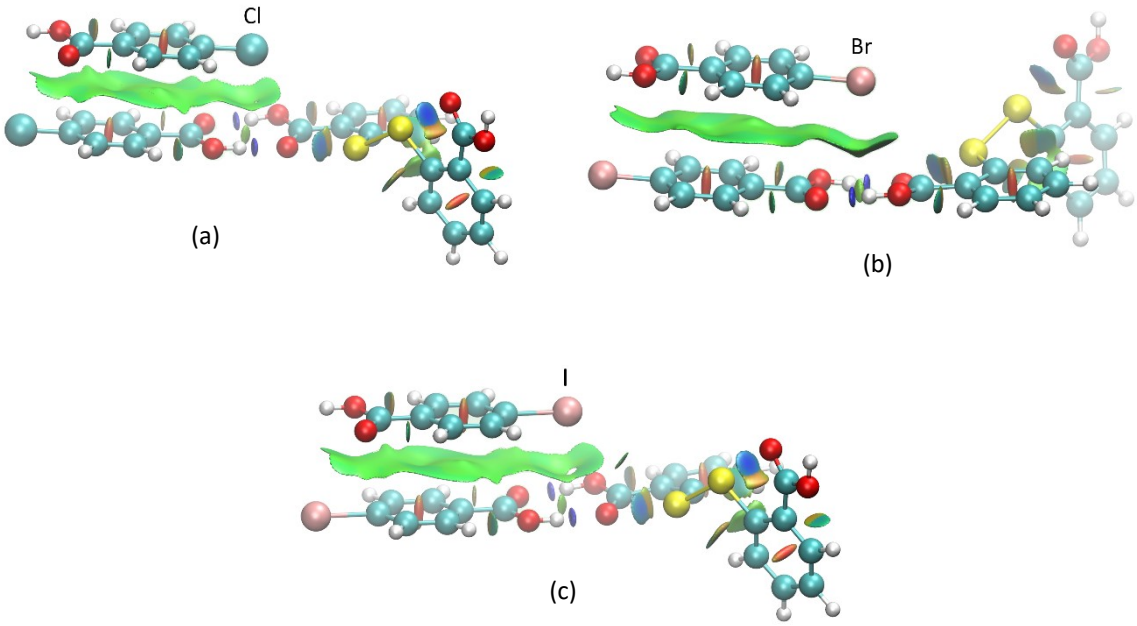

ESI Figure 13. Non-covalent interaction (NCI) plot showing the iso-surface of the reduced density gradient resulting from the C–X···quasi-π[{···HOC=O}$_2$] interaction for (a) X = Cl, (b) X = Br and (c) X = I. The iso-surfaces are coloured according to the values of electron density, with green indicative of weak attraction, while blue and red are indicative of strong attraction and strong repulsion, respectively. The cut-off value is set at RDG = 0.5 a.u. and colour scale is within -0.4 < ρ < 0.4 a.u..

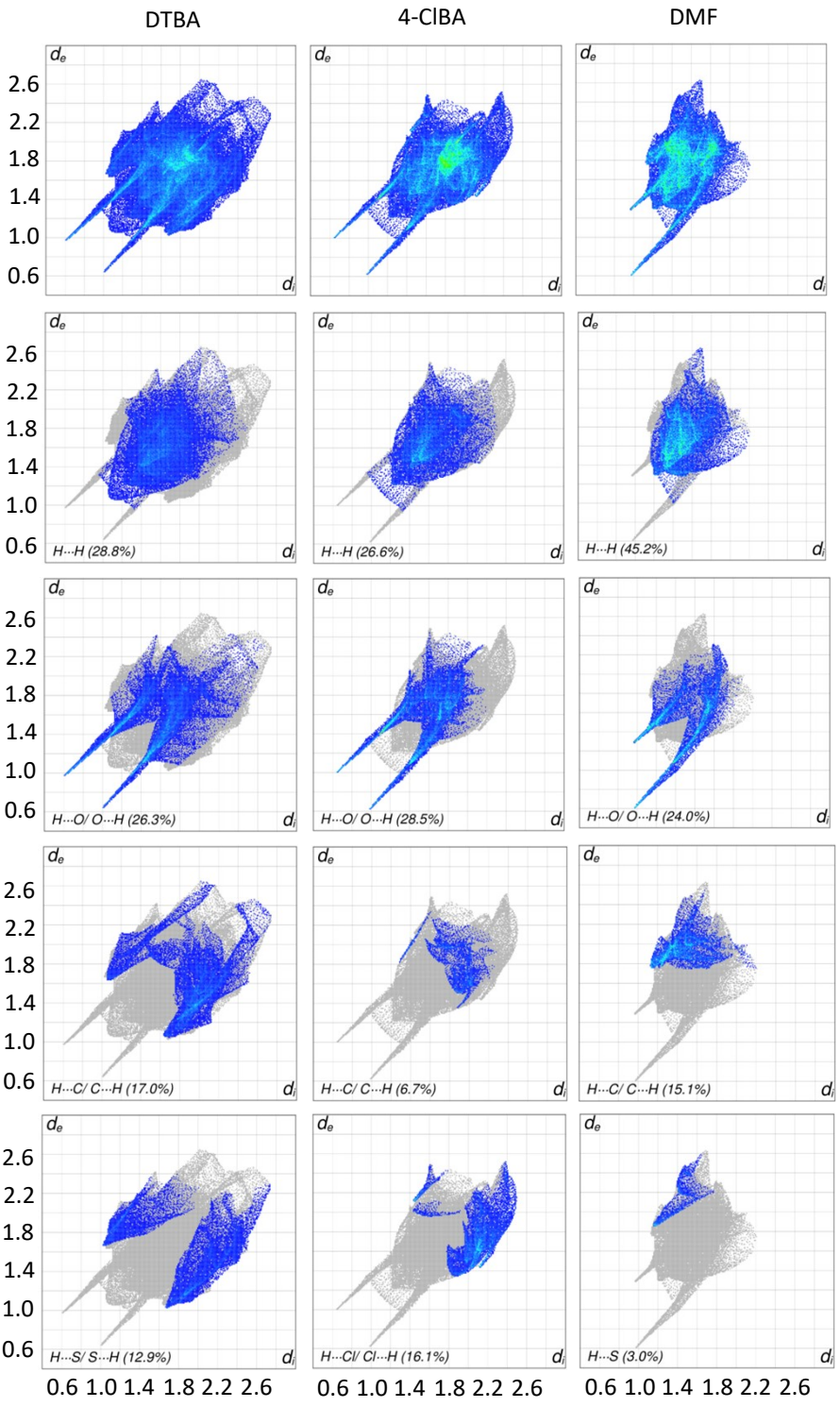
DTBA
4-ClBA
DMF
d_e
d_i
2.6
2.2
1.8
1.4
1.0
0.6
H···H (28.8%)
H···H (26.6%)
H···H (45.2%)
H···O/ O···H (26.3%)
H···O/ O···H (28.5%)
H···O/ O···H (24.0%)
H···C/ C···H (17.0%)
H···C/ C···H (6.7%)
H···C/ C···H (15.1%)
H···S/ S···H (12.9%)
H···Cl/ Cl···H (16.1%)
H···S (3.0%)
0.6 1.0 1.4 1.8 2.2 2.6
0.6 1.0 1.4 1.8 2.2 2.6
0.6 1.0 1.4 1.8 2.2 2.6

(a)

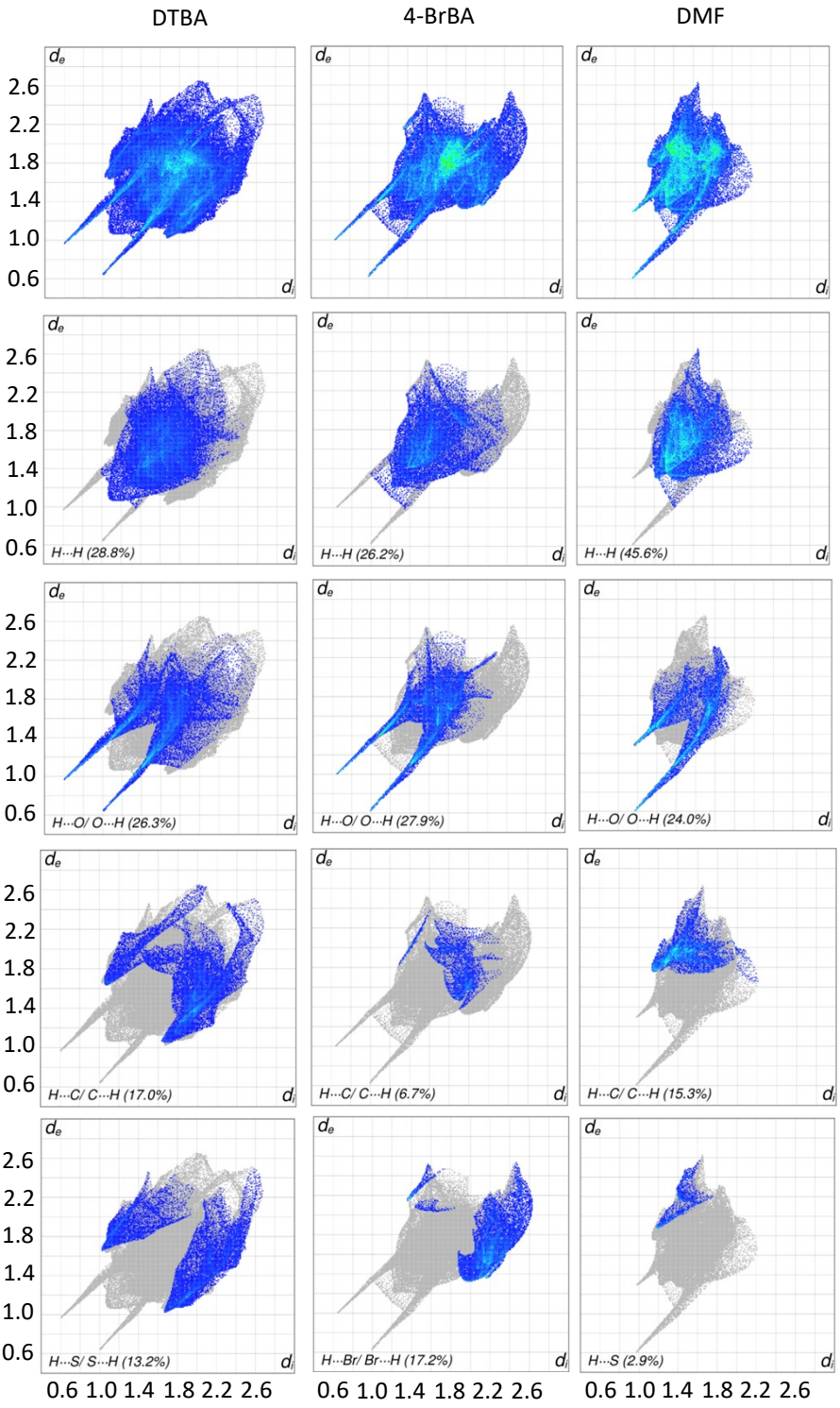
DTBA
4-BrBA
DMF
d_e
d_i
2.6
2.2
1.8
1.4
1.0
0.6
H···H (28.8%)
H···H (26.2%)
H···H (45.6%)
H···O/ O···H (26.3%)
H···O/ O···H (27.9%)
H···O/ O···H (24.0%)
H···C/ C···H (17.0%)
H···C/ C···H (6.7%)
H···C/ C···H (15.3%)
H···S/ S···H (13.2%)
H···Br/ Br···H (17.2%)
H···S (2.9%)
0.6 1.0 1.4 1.8 2.2 2.6
0.6 1.0 1.4 1.8 2.2 2.6
0.6 1.0 1.4 1.8 2.2 2.6

(b)

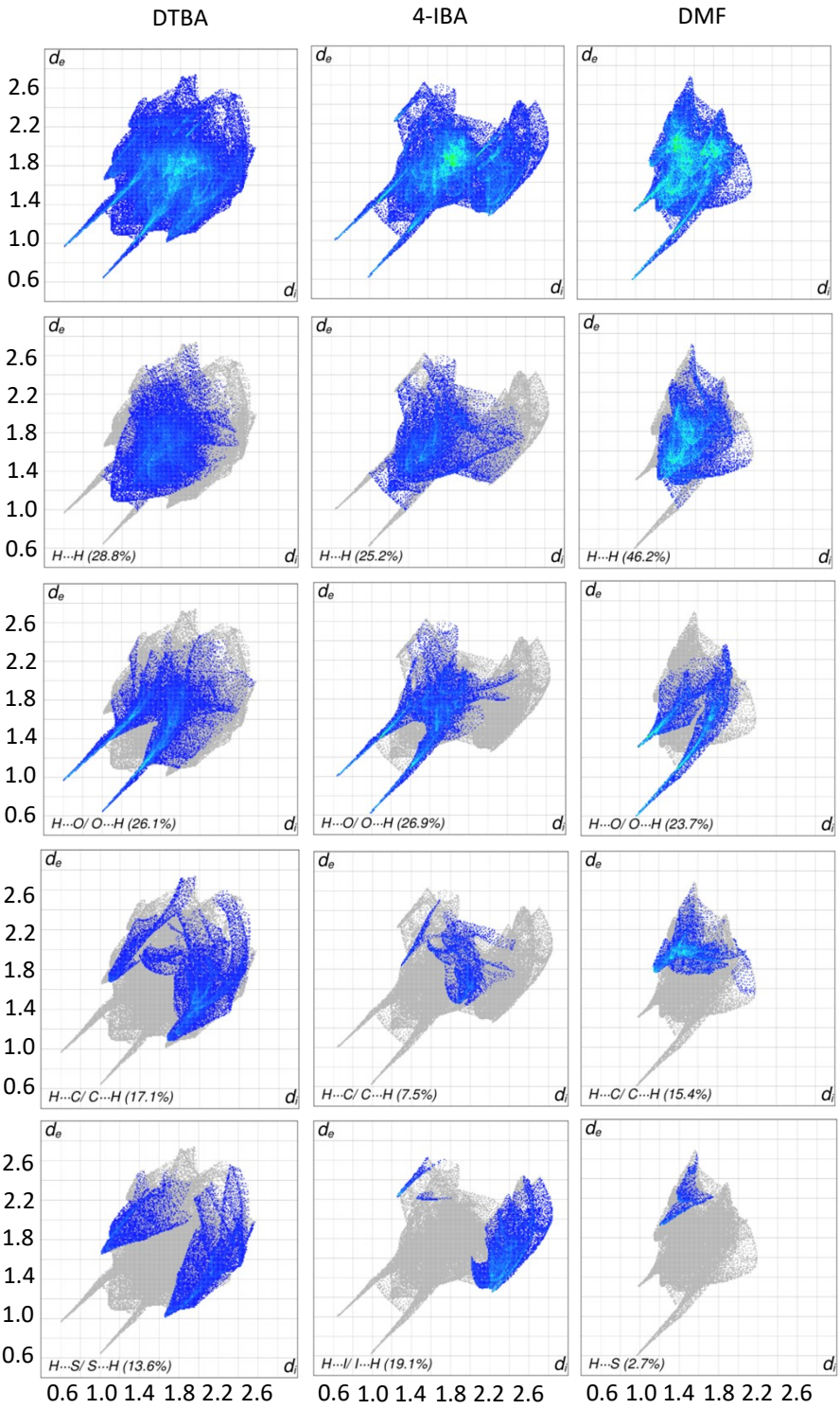

(c)

ESI Figure 14. Overall (top) and decomposed fingerprint (H···H, H···O/O···H, H···C/C···H and H···S/S···H) plots delineated into the corresponding specific contacts for the individual components in (a) **1**, (b) **2** and (c) **3**.

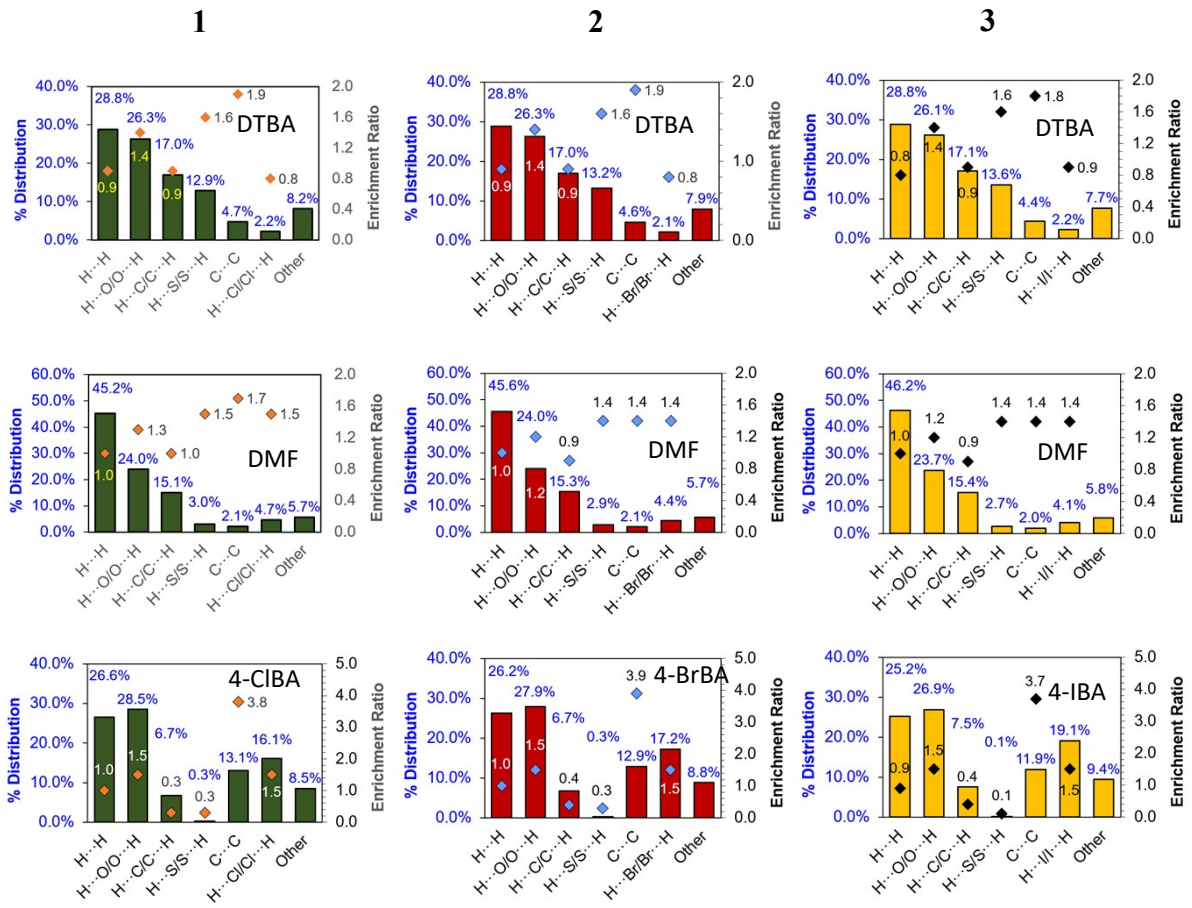

ESI Figure 15. The distribution of calculated surface contacts and associated enrichment ratios for the individual components (rows) of **1**-**3** (columns).

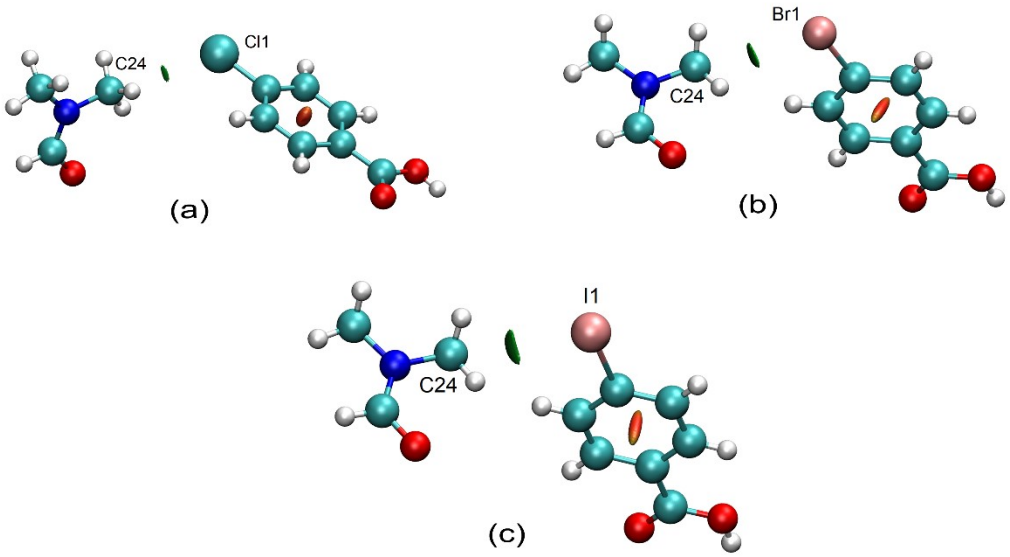

ESI Figure 16. Non-covalent interaction (NCI) plot showing the iso-surface of the reduced density gradient resulting from the C24···X interactions in (a) **1**, (b) **2** and (c) **3**. The iso-surface is coloured according to the values of electron density, with green indicative of weak attraction, while blue and red are indicative of strong attraction and strong repulsion, respectively. The cut-off value is set at RDG = 0.5 a.u. and colour scale is within $-0.4 < \rho < 0.4$ a.u.

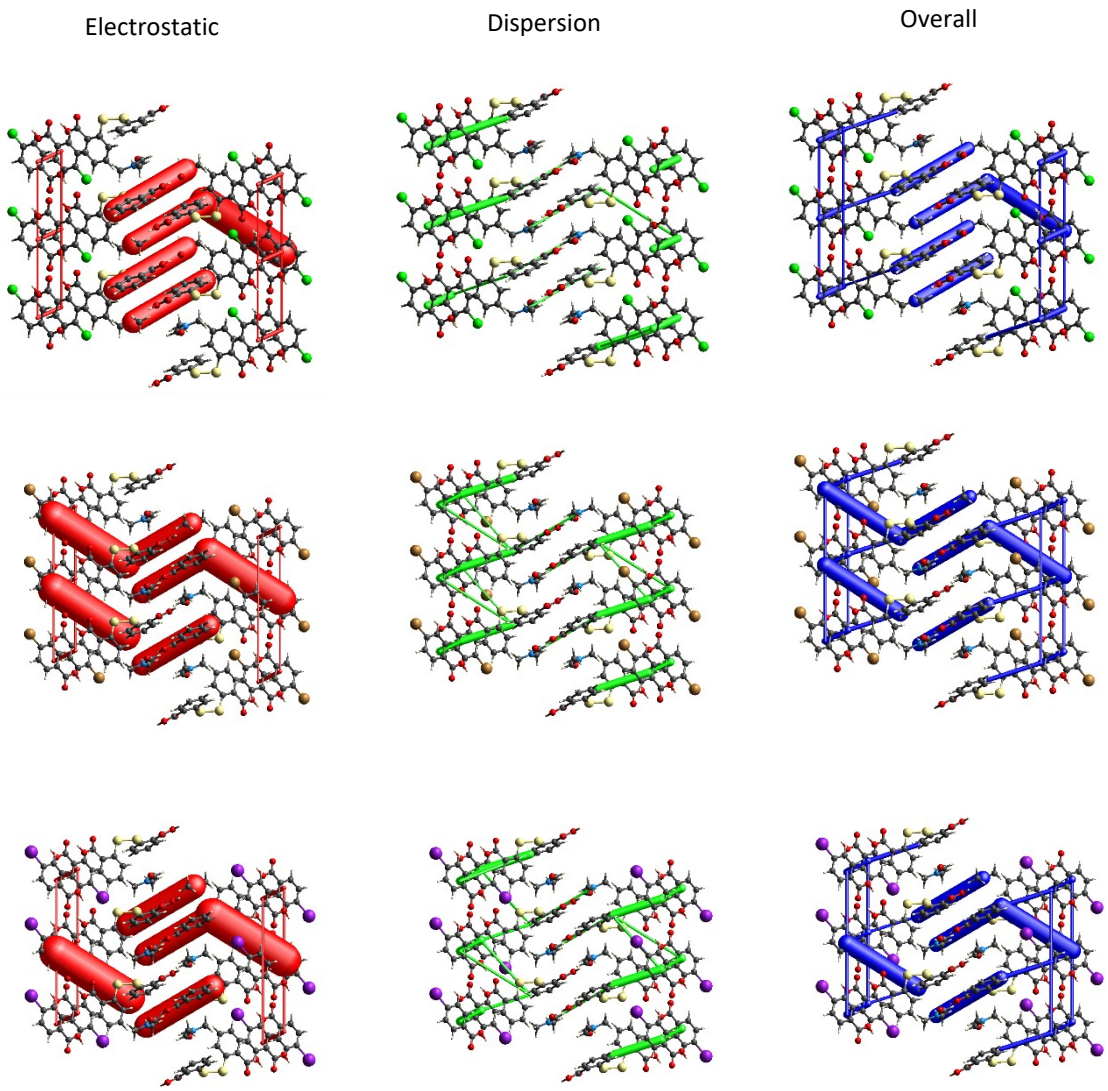

ESI Figure 17. Perspective views of the electrostatic energy framework (left column), dispersion force (middle column) and overall energy framework (right column) for **1** (top row), **2** (middle row) and **3** (bottom row). The cylindrical radius is proportional to the relative strength of the corresponding energies and adjusted to the same scale factor of 100 with a cut-off value of 8 kJ/mol within a 2 × 2 × 1 unit-cells.